PERGAMON

Atmospheric Environment 34 (2000) 781–792

ATMOSPHERIC ENVIRONMENT

www.elsevier.com/locate/atmosenv

Application of Bayesian Monte Carlo analysis to a Lagrangian photochemical air quality model

Michelle S. Bergin[1], Jana B. Milford*

Department of Mechanical Engineering, University of Colorado, Boulder, CO 80309-0427, USA

Received 8 February 1999; accepted 12 July 1999

Abstract

Uncertainties in ozone concentrations predicted with a Lagrangian photochemical air quality model have been estimated using Bayesian Monte Carlo (BMC) analysis. Bayesian Monte Carlo analysis provides a means of combining subjective "prior" uncertainty estimates developed by standard Monte Carlo techniques with information about the agreement between model outputs and observations. The resulting "posterior" uncertainty estimates reflect both the model's performance and subjective judgments about uncertainties in model parameters and inputs. To demonstrate the approach, BMC analysis was applied to a model of ozone concentrations along two-day trajectories ending on 28 August 1987 at Azusa and Riverside, CA. Refined estimates of uncertainties in base case O_3 concentrations were calculated, along with estimates of uncertainties in the response to 25% reductions in motor vehicle emissions of nitrogen oxides and volatile organic compounds. For the cases studied, the model results were in reasonable agreement with spatially interpolated observations. Bayesian updating reduced the estimated uncertainty in predicted peak O_3 concentrations from 35 to 20% at Azusa and from 24 to 18% at Riverside.

Keywords: Urban ozone; Air quality modeling; Uncertainty analysis

1. Introduction

Photochemical air quality models are used to assess the effects of proposed control strategies for urban ozone. The models combine mathematical descriptions of atmospheric physics and chemistry, accounting for emissions, transport, reactions, and deposition. Uncertainties in the input data, assumptions, and other aspects of the models need to be quantified in order to help identify robust control strategies. Previous studies have estimated uncertainties in photochemical air quality model results by using Monte Carlo analysis or other techniques to propagate estimates of uncertainties in model parameters and inputs (Bergin et al., 1999; Pun, 1998; Hanna et al., 1998; Gao et al., 1996; Yang et al., 1995). However, the resulting uncertainty estimates do not directly account for the performance of the models as evaluated against observations (McRae and Seinfeld, 1983; Tesche, 1988). In standard Monte Carlo studies, model results that match the observations and those in poor agreement with them are treated as equally probable. In contrast, Bayesian Monte Carlo (BMC) analysis provides a means of adjusting uncertainty estimates to reflect model performance.

In standard Monte Carlo analysis, statistical techniques or subjective judgments are used to assign probability distribution functions to model parameters and inputs. Hundreds of model simulations are then run, using randomly sampled values of each uncertain parameter. A common modification of standard Monte Carlo analysis is to use stratified sampling schemes such as Latin hypercube sampling (LHS: Iman and Shortencarier, 1984), rather than random sampling, for computational efficiency. With Monte Carlo analysis, some combinations of input and parameter values can lead to "suspect" model results, in the sense that they differ

[1] Currently at the Georgia Institute of Technology, Department of Civil and Environmental Engineering, Atlanta, GA 30332, USA.

* Corresponding author.

1352-2310/00/$ - see front matter
PII: S1352-2310(99)00346-5

significantly from observations. This problem has been addressed in water quality modeling studies by discarding simulations that fall outside a specified limit for agreement with the observations (e.g., Hornberger and Spear, 1980; Beck, 1987). Dilks et al. (1992) proposed Bayesian Monte Carlo analysis for use in water quality modeling as an improvement over such binary schemes for acceptance or rejection.

Bayesian Monte Carlo analysis refines uncertainty estimates by using a continuous likelihood function to weight the results of individual Monte Carlo simulations. The likelihood function quantifies the probability of obtaining a specified difference between model results and observations, accounting for the errors in the observations. Through the likelihood function, the highest probability is assigned to those Monte Carlo runs that most closely match the observations, with relatively little weight given to runs that produce a poor fit. BMC can be used to refine estimates for model parameters, identifying and accounting for covariances between them. BMC also provides a means of accounting for model performance as well as input uncertainties in developing estimates of uncertainty in model predictions, e.g., for control scenarios.

BMC has been applied to estimate uncertainties in potential sea level rise due to climate change (Patwardhan and Small, 1992), environmental health risk assessment (Brand and Small, 1995), groundwater modeling (Sohn et al., 1999) and to evaluate the expected value of sample information with respect to surface water sediment contamination (Dakins et al., 1996). Romanowicz et al. (1998) applied BMC to a Gaussian plume air quality model used to simulate SF_6 tracer experiments, with roughness length, wind speed at 10 m and the wind speed profile treated as uncertain input parameters. In addition, Pun (1998) has discussed the use of field observations to help assess uncertainties in photochemical air quality models.

This study incorporates interpolated measurements of O_3 concentrations with results from a previous Monte Carlo uncertainty analysis (Bergin et al., 1999). In the previous study, the vertically resolved trajectory version of the California/Carnegie Institute of Technology (CIT) air quality model (Russell et al., 1983; Pandis et al., 1992) was used with Monte Carlo analysis to quantify uncertainties in model results, accounting for uncertainties in 51 inputs or parameters. Using these Monte Carlo results as "prior" uncertainty estimates, the current study derives "posterior" uncertainty estimates for both model inputs and outputs by applying Bayes' Theorem to incorporate information on model performance.

2. Methods

The BMC approach is used here to determine the posterior probabilities of individual simulations in a Monte Carlo analysis. From Bayes' theorem, the posterior probability of model output Y_k from simulation k is defined as (Brand and Small, 1995)

$$p'_k = p(Y_k|O) = \frac{L(Y_k|O)p(Y_k)}{\sum_{j=1}^{N} L(Y_j|O)p(Y_j)}, \quad (1)$$

where $p(Y_k) = p_k$ is the prior probability of the kth run out of $j = 1, \ldots, N$ runs. The likelihood, $L(Y_k|O) = p(O|Y_k)$ is the probability of observing value O given that the model output Y_k is the true value. The prior probability of each Monte Carlo simulation is equal to $1/N$. The resulting posterior (updated) distribution for output variable Y has a mean of

$$\mu'_Y = \sum_{j=1}^{N} (Y_j \times p'_j), \quad (2)$$

and standard deviation of

$$\sigma'_Y = \sqrt{\sum_{j=1}^{N} (Y_j - \mu'_Y)^2 p'_j}. \quad (3)$$

The posterior probabilities, p', developed from the base case model outputs can also be applied to update estimates of sampled input parameter values or of model predictions such as control scenario results. This is done by substituting the values of the parameters, inputs or predictions in each run for values of Y in Eqs. (2) and (3). Finally, the posterior correlation between output Y and input parameter X_i is

$$\rho'_{Y,X_i} = \frac{\sum_{j=1}^{N} (Y_j - \mu'_Y)(X_{i,j} - \mu'_{X_i})p'_j}{\sigma'_Y \sigma'_{X_i}}. \quad (4)$$

Eq. (4) can also be used to calculate posterior correlations between pairs of input parameters.

Eq. (1) requires both a set of Monte Carlo simulations and a corresponding set of observations. Also, an estimate must be made of what the best possible agreement could be between the model results and observations, which is quantified by the likelihood function. The formulations of the likelihood functions used in this analysis are discussed below, following presentation of the air quality model and Monte Carlo calculations used to evaluate the prior uncertainties.

The prior distributions used here are from a Monte Carlo modeling study by Bergin et al. (1999). They applied Monte Carlo analysis with LHS to evaluate the effects of uncertainties in 51 model parameters on output concentrations of ozone and other secondary compounds. Effects of uncertainties on model predictions of the response of peak O_3 to 25% reductions in motor vehicle emissions of nonmethane organic compounds (NMOC) and nitrogen oxides (NO_x) were also evaluated. Here, Bayesian updates are made for two of the sets of trajectories modeled by Bergin et al., which end at Riverside and Azusa (see Fig. 1) at the times at which peak O_3 concentrations were measured on 28 August 1987.

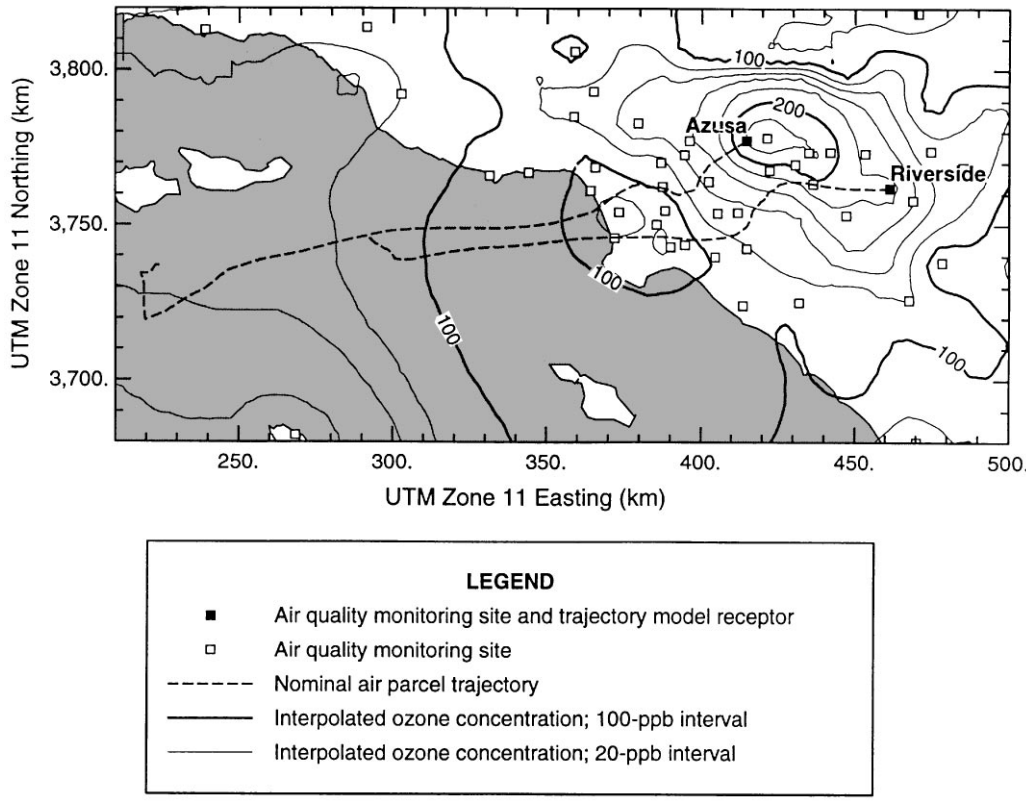

Fig. 1. Air quality monitoring sites and contours of interpolated ozone concentrations at 1:30 p.m. on 28 August 1987. The paths of the nominal air parcel trajectories arriving at Azusa at 1:30 p.m. and Riverside at 2:30 p.m. are superimposed on the figure.

For each simulation, the trajectory version of the CIT model simulates a parcel of air traveling across an airshed by solving the Lagrangian formulation of the atmospheric diffusion equation

$$\frac{\partial C_i}{\partial t} = \frac{\partial}{\partial z}\left(K_{zz}\frac{\partial C_i}{\partial z}\right) + R_i(\underline{C}), \quad i = 1, \ldots, n, \tag{5}$$

where C_i is the ensemble mean concentration of species i, K_{zz} is the turbulent eddy diffusivity in the vertical direction, z, and $R_i(\underline{C})$ is the net rate of generation of species i by chemical reactions. The initial condition is $C_i(z, 0) = C_i^0(z)$, and the boundary conditions are

$$v_g^i C_i - K_{zz}\frac{\partial C_i}{\partial z} = E_i, \quad \text{at the surface,}$$

and

$$K_{zz}\frac{\partial C_i}{\partial z} = 0 \quad \text{at the top of the column.}$$

Here, v_g^i is the surface deposition velocity and E_i is the surface emissions flux of species i. The trajectory column modeled in this study is comprised of five vertical layers. The most significant limitations of the trajectory formulation are its inability to account for horizontal diffusion and wind shear. Nevertheless, the trajectory version of the CIT model was used because it accounts for more physical detail than a box model, while remaining computationally tractable in the context of the hundreds of model runs required for Monte Carlo analysis.

The trajectory model incorporates the Statewide Air Pollution Research Center 1993 (SAPRC93) chemical mechanism (Carter, 1995) and was applied to the 27–28 August 1987 episode of the South Coast air quality study (SCAQS; Lawson, 1990). Emissions inputs for stationary source and off-road mobile sources were obtained from the California Air Resources Board and the South Coast Air Quality Management District. On-road motor vehicle emissions were estimated using a fuel-based approach (Harley et al., 1997).

Bergin et al. (1999) considered uncertainty in wind speed and direction, and in chemical rate constants, deposition affinities, mixing heights, the atmospheric stability class, and emissions. Table 1 provides a list of the inputs and parameters that were treated as random

Table 1
Distributions of random variables included in Monte Carlo analysis (Bergin et al., 1999)[a]

Parameter label	Description	COV[b]
Air parcel trajectory	Sum of CO emissions along each trajectory	
CO_traj	Azusa	0.122
	Riverside	0.146
Pollutant emissions		
MV_emis	Motor vehicle emissions[c] (applied to CO, NO_x, and NMOC)	0.246
MV_NO_x	Motor vehicle NO_x (applied to NO_x only)	0.06
MV_NMOC	Motor vehicle NMOC (applied to NMOC only)	0.06
Othr_NO_x	Other anthropogenic NO_x	0.149
Othr_NMOC	Other anthropogenic NMOC	0.294
Biog_emis	Biogenic hydrocarbons: α-pinene, isoprene, higher lumped alkenes (OLE3)	0.385
Chemistry: reaction rate constants		
$NO + O_3$	$NO + O_3 \rightarrow NO_2 + O_2$	0.095
$O(1D) + H_2O$	$O(^1D). + H_2O \rightarrow 2\ OH.$	0.183
$O(1D) + M$	$O(^1D). + M \rightarrow O(^3P). + M$	0.183
$CO + OH$	$CO + OH. \rightarrow HO_2. + CO_2$	0.265
$HO_2 + NO$	$HO_2. + NO \rightarrow OH. + NO_2$	0.183
RCO3 + NO[d]	$RCO3. + NO \rightarrow NO$	0.343
RCO3 + NO_2[e,f]	$RCO3. + NO_2 \rightarrow NO_2$	0.150
RO2R + NO[g]	$RO2R. + NO \rightarrow NO_2 + HO_2.$	0.417
RCHO + *hv*	$RCHO + hv \rightarrow CCHO + RO2R. + RO2. + CO + HO_2.$	0.343
PPN	$PPN \rightarrow C2CO\text{-}O_2. + NO_2 + RCO3$	0.804
ALK2 + OH	[lumped alkanes] + OH. → products	0.265
ARO2 + OH	[lumped aromatics] + OH. → products	0.265
OLE2 + OH	[lumped alkenes] + OH. → products	0.183
OLE2 + O_3	[lumped alkenes] + O_3 → products	0.417
$NO_2 + hv$	$NO_2 + hv \rightarrow NO + O(^3P).$	0.183
$O_3 + hv$	$O_3 + hv \rightarrow O(^1D). + O_2$	0.265
AFG2 + *hv*[h]	[aromatic fragmentation products] + *hv* → products	1.333
HCHO + *hv*[i]	$HCHO + hv \rightarrow 2\ HO_2. + CO$	0.343
NO_2 + OH[f]	$NO_2 + OH. \rightarrow HNO_3$	0.265
ETHE + OH[f]	$ETHE + OH. \rightarrow RO2R. + RO2. + 1.56HCHO + 0.22CCHO$	0.114
PAN	$PAN \rightarrow CCO\text{-}O_2. + NO_2 + RCO3.$	0.385
Mixing heights		
MH_xxxx	Mixing height for period ending at time xxxx; 11 periods are represented, from 0 to 2400 minutes.	See Bergin et al. (1999)
Deposition[j]		
O_3_aff	O_3 deposition affinity	0.29
NO_aff	NO deposition affinity	0.29
NO_2_aff	NO_2 deposition affinity	0.29
Atmospheric stability		
Pas_Gif[k]	Pasquill–Gifford classification	0.11

[a]Distributions are treated as independent and lognormal with a mean of 1.0 unless noted otherwise. See Bergin et al. (1999) for references and further details.

[b]Coefficient of variation (COV) = standard deviation normalized by nominal value at 298 K and 1 atmosphere.

[c]Uncertainty due to variability in remote sensing of CO emissions (see Bergin et al., 1999; Harley et al., 1997, for elaboration).

[d]Correlated ($\rho = 1$) with rate constants for $CCO\text{-}O_2. + NO \rightarrow CO_2 + NO_2 + HCHO + RO2R. + RO2.$; $C2COO2. + NO \rightarrow CO_2 + NO_2 + CCHO + RO2R. + RO2.$; and for other peroxyacyl radical reactions with NO_2.

[e]Correlated ($\rho = 1$) with rate constants for $CCO\text{-}O_2. + NO_2 \rightarrow PAN$; $C2COO2. + NO_2 \rightarrow PPN$; and rate constants for other peroxyacyl radical reactions with NO_2.

[f]Coefficient of variation calculated from Troe parameter uncertainty estimates.

[g]Correlated ($\rho = 1$) with rate constants for $R2O2 + NO \rightarrow NO_2$; $RO2 + NO \rightarrow NO$; and for other peroxy radical reactions with NO.

[h]Correlated ($\rho = 1$) with rate constant for $AFG1 + hv \rightarrow HO_2. + HCOCO\text{-}O_2. + RCO3.$

[i]Correlated ($\rho = 1$) with rate constant for $HCHO + hv \rightarrow H_2 + CO$.

[j]Deposition affinity distributions are assumed to be uniform.

[k]The Pasquill–Gifford distributions are discrete, and are described in detail by Bergin et al. (1999).

variables. Ensembles of trajectories were generated by adding random deviations in the winds at each hour as the trajectories are propagated backwards from the air quality monitoring sites (Noblet et al., 1998). For purposes of estimating uncertainty contributions, each trajectory path in the ensemble is represented by the sum of the CO emissions along the path, which in turn is highly correlated with NO_x and NMOC emissions. Bergin et al. (1999) neglected uncertainties in the other rate parameters of the SAPRC93 mechanism, temperature, relative humidity, and the initial concentrations of O_3, NMOC, and NO_x, because preliminary sensitivity calculations showed they had little effect on peak ozone concentrations. Two hundred simulations were performed for each trajectory endpoint, each having a prior probability of $\frac{1}{200}$, and each incorporating a unique trajectory path and set of input values sampled with LHS. Of note, the uncertainties in model inputs (other than the trajectory path) were treated as multiplicative factors, allowing the same 200 sets of sample values to be used for both trajectory endpoints. Bergin et al. (1999) give a complete description of the uncertain parameters and the basis for their estimated probability distributions.

In typical air quality applications, observations of pollutant concentrations are point measurements while model results are averaged over a grid cell volume. However, pollutant concentrations have spatial inhomogeneities within the volumes represented by model grid cells. McNair et al. (1996) have argued that if the network of measurements is reasonably dense, an air quality model cannot be expected to produce a concentration field that matches pollutant measurements at discrete points any better than a field produced by directly interpolating the measurements over the model grid. Adopting this argument, the model results in this study are compared to interpolated observations, with the likelihood functions reflecting the interpolation errors.

For use in the Bayesian analysis, O_3 measurements from 56 SCAQS monitoring stations were averaged for each hour of the two-day simulation period and interpolated to obtain two-dimensional gridded fields of O_3 concentrations (Harley, 1998; Goodin et al., 1979). Interpolated ozone concentrations along the nominal trajectories used by Bergin et al. (1999) were read from the fields by projecting the trajectory positions onto the successive, hourly windfields. The resulting arrays of O_3 concentrations were used in the likelihood calculations.

McNair et al. (1996) used a data withholding technique to compare observed and interpolated O_3 concentrations for 37 of the SCAQS monitoring stations, for the pollution episode and area used in this study. Interpolated fields were constructed with data withheld from each monitoring site in turn, so the resulting interpolation error could be calculated at each site. McNair et al. reported a normalized root-mean-square (RMS) error of $\sim 30\%$ with a bias of -7% between interpolated and observed ozone concentrations above 60 ppb, for 28 August 1987. The RMS error was used in the BMC calculations as an estimate of the standard deviation of the error associated with the interpolated concentrations. The -7% bias is not considered in the BMC calculations, because we view it as a legitimate correction for the mismatch between point measurements and spatially averaged model results.

For this study, the data withholding results of McNair et al. (1996) were also examined to determine whether the interpolation errors were serially or spatially correlated. Based on this analysis, trajectories ending at Riverside and Azusa were selected to demonstrate the BMC approach. Interpolation errors were not significantly correlated across these two sites, making it easier to define and calculate appropriate likelihood functions. However, over the time period from 6 a.m. to 2 p.m., and over the set of 37 SCAQS monitoring sites, the average 1-h lag autocorrelation coefficient for the error was about 0.5. This degree of autocorrelation was accounted for in calculating a likelihood function that utilized the 5 h of O_3 concentrations preceding the observed O_3 peak along the Azusa and Riverside trajectories, as discussed below.

Two sets of likelihood functions (and therefore posterior probabilities) were calculated, one based on the final interpolated O_3 concentrations at the two sites and the other on the interpolated concentrations for the last five hours along each trajectory. Results from the two sites are combined because the best estimates of model parameters (e.g., rate constants) should be the same for both locations. With the assumption that the errors in the interpolated concentrations at Azusa and Riverside are independent and normally distributed with mean of zero, the "final-h" likelihood is calculated from

$$L(Y_k|O) = \frac{1}{\sqrt{2\pi}\sigma_\varepsilon} \exp\left(-\frac{1}{2}\left[\frac{O - Y_k}{\sigma_\varepsilon}\right]^2\right). \tag{6}$$

In (6), O is the interpolated observed O_3 concentration, Y_k is the output concentration from the kth simulation and σ_ε is the standard deviation of the error in the interpolated observations. Based on McNair et al.'s study, σ_ε is taken as $0.3\,O$. Combining the results and data from the two sites, the likelihood for the kth simulation is

$$L(Y_k|O_{\mathrm{Az}})L(Y_k|O_{\mathrm{Ri}}), \tag{7}$$

where Az denotes Azusa and Ri denotes Riverside.

Likelihoods were also calculated for 5 h time series along each trajectory by viewing the series of errors in interpolated ozone concentrations as a Markov sequence (Benjamin and Cornell, 1970), in which each value is assumed to be correlated only with the previous value

(Chock, 1984). With this assumption, the bivariate normal probability distribution (Guttman et al., 1982) can be used to derive a Markov-chain likelihood function as

$$L(Y_k|\boldsymbol{O}) = \prod_{m=1}^{H} \frac{1}{2\pi(1-\rho^2)\sigma_{\varepsilon,m+1}} \times \exp\left(-\frac{1}{2\sigma_{\varepsilon,m+1}^2(1-\rho^2)} \times \left[w_{m+1,k} - \mu_{m+1} - \rho\frac{\sigma_{\varepsilon,m+1}}{\sigma_m}(w_{m.k} - \mu_m) \right]^2 \right). \quad (8)$$

Here, $\boldsymbol{O}$ is a vector of sequential observations made at equal time intervals, H is the total number of observations; $\sigma_{\varepsilon,m}$ is the standard deviation of the error in the observations at the mth observation time; ρ is the autocorrelation coefficient, and $w_{m,k} = (O_m - Y_{m,k})$ for simulation k and time step m. The mean value of $w_{m,k}$, i.e., μ_m, is assumed to be zero. The value of $\sigma_{\varepsilon,m}$ is taken as 0.3 O_m. For this study, a "5 h" likelihood function was defined using Eq. (8) by selecting $H = 5$, with observations at hourly intervals, and setting $\rho = 0.5$. Likelihood functions calculated separately for the Azusa and Riverside trajectories were combined according to Eq. (7).

A 5 h period at the end of each trajectory was selected for the second likelihood function because it captures the daytime rise to the peak O_3 concentration. In addition, it avoids periods when observations drop below the 60 ppb cutoff that McNair et al. (1996) used in calculating the RMS interpolation error. Use of a multi-hour time series is also in keeping with the proposed 8-h averaging time for the National Ambient Air Quality Standard for O_3. Posterior estimates based on the 5-h likelihood function incorporate more information from the observations and thus should be preferred to those calculated using only the final concentration. However, for comparison both sets of posterior estimates are presented in the next section.

3. Results

Fig. 1 shows the interpolated ozone isopleths for 1:30 p.m. on 28 August together with nominal trajectory paths leading to Azusa and Riverside. Note, the trajectory paths actually represent steps in time as well as location, while the isopleths are presented for a single 1 h averaged period. The interpolated observations are shown for 1:30 p.m. because the peak O_3 concentration at Azusa was measured then. The peak O_3 concentration at Riverside was observed at 2:30 p.m. The interpolated values over the ocean are highly uncertain due to lack of observations there, but in any case are not used in the Bayesian analysis.

Time series of O_3 concentrations along trajectories leading to Azusa and Riverside are shown in Fig. 2, comparing interpolated measurements with prior Monte Carlo modeling results from Bergin et al. (1999). The time series are excerpts from the full two-day trajectories, starting at 4 a.m. on the 28th and ending at the time of the observed peak at each location. In each case the error bars represent $\pm 1\sigma$. At both sites, the prior mean concentrations from the Monte Carlo simulations exceed the interpolated, observed O_3 concentrations from the time of sunrise until almost the final hour, at which time the interpolated observations exceed the model results. The uncertainty in the prior modeled O_3 concentrations is also larger than the assumed 30% interpolation error until almost the final hour. However, for the final O_3 concentration at Riverside, the estimated error in the interpolated observations is greater than the prior uncertainty from the Monte Carlo results. At Azusa, the prior uncertainty in the final modeled O_3 concentration is similar to the interpolation error.

The comparison shown in Fig. 2 suggests that the two likelihood functions developed for the Bayesian Monte Carlo analysis should give somewhat different results. The likelihood function based only on the final O_3 concentrations is expected to give approximately equal weight to the prior and the interpolated values because their errors are approximately equal, and to produce a posterior mean that is somewhat higher than the prior mean. In contrast, because the observations have smaller errors than the model results up until the final hour, the likelihood function based on the 5-h time series is expected to give more weight to the observations, and result in a posterior mean that is lower than the prior estimate.

Final O_3 concentrations are presented in Table 2, comparing the observed point measurements with the interpolated values, and comparing prior Monte Carlo results with posterior probabilities calculated from both final and 5-h likelihood functions. Results of a simulation using nominal values of all of the parameters and inputs are also shown for each site. The interpolated O_3 concentrations are lower than observed concentrations at both sites. Use of the final-h likelihood function increases the mean estimates of the final O_3 concentrations at both sites by about 50% of the difference between the prior means and the interpolated values. The posterior mean final concentrations estimated using the 5-h likelihood function are lower than the prior means at both sites, reflecting the fact that the interpolated observations are lower than the prior mean estimates over the four previous hours. With both likelihood functions the posterior standard deviations in the final O_3 concentrations are reduced from the prior standard deviations. For Azusa, the posterior uncertainties in the final O_3 concentration (100% × standard deviation/mean) are about 20%, whereas the prior uncertainty was 35%. For Riverside, the uncertainty is reduced from the prior estimate of 24% to posterior estimates of about 18%.

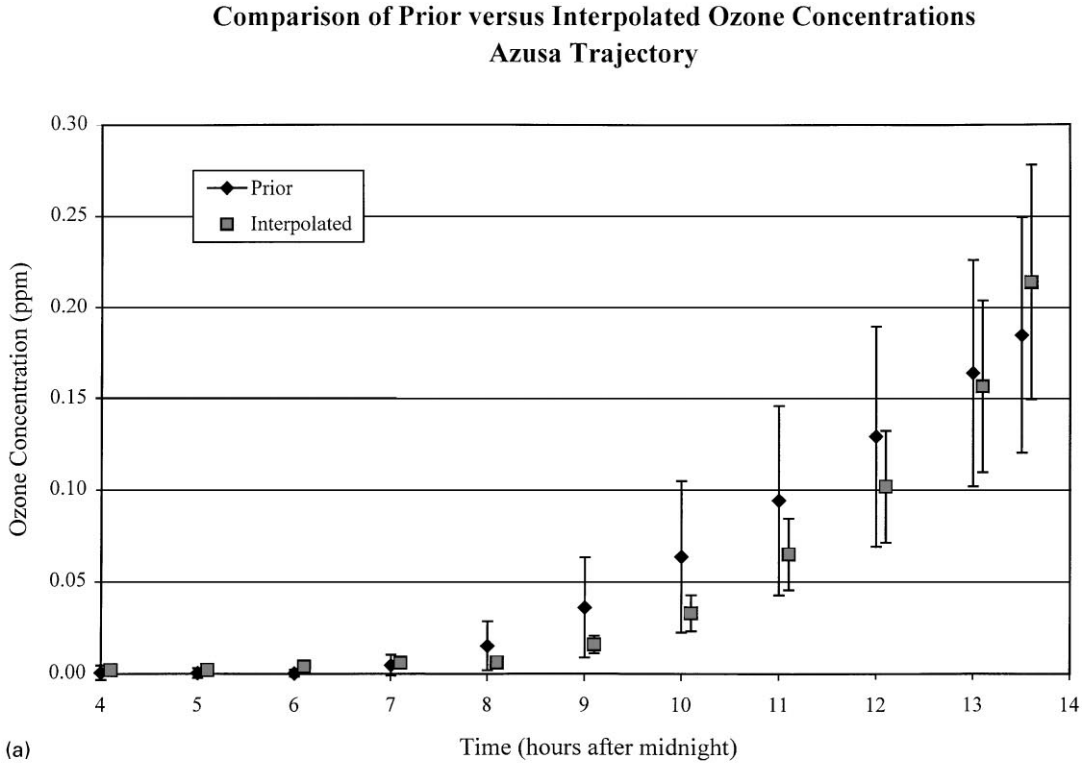

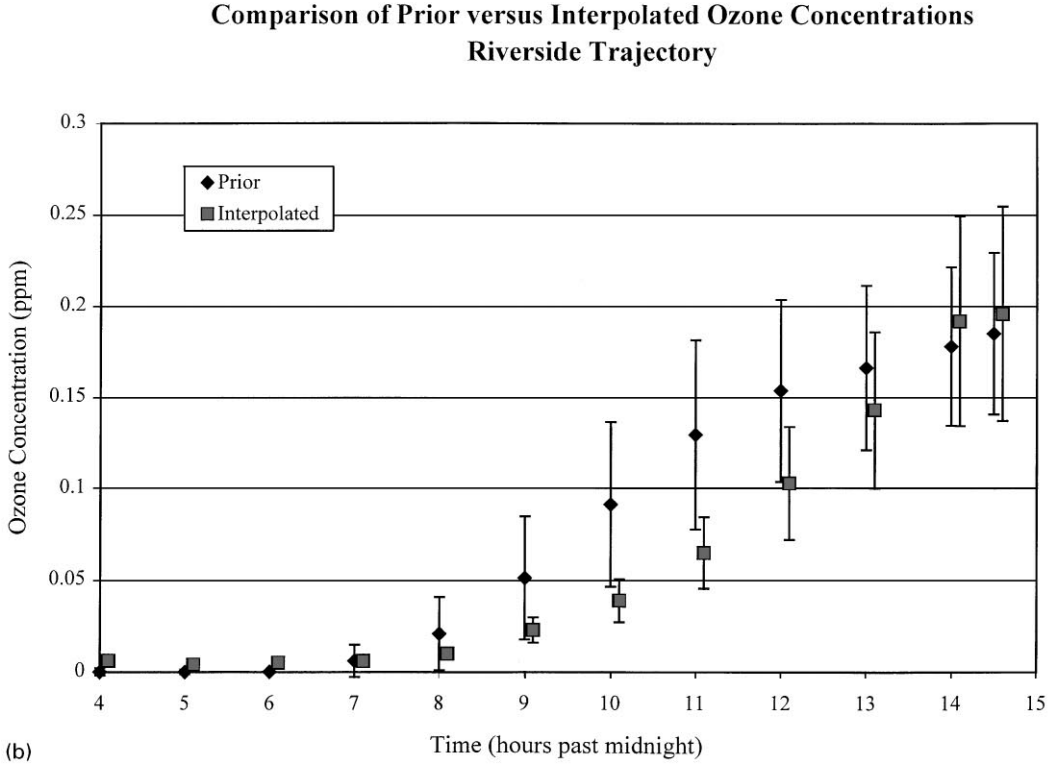

Fig. 2. Comparison of ozone concentrations from prior Monte Carlo modeling (Bergin et al., 1999) versus interpolated observations along (a) the Azusa trajectory and (b) the Riverside trajectory. The mean value and mean $\pm 1\sigma$ are shown for each case.

Table 2
Comparison of peak observed, interpolated and modeled ozone concentrations (ppm) for Azusa at 1:30 p.m. and Riverside at 2:30 p.m. on August 28, 1987

Site	Observed	Interpolated observation	Nominal model result	Prior Monte Carlo mean $\pm 1\sigma$	Final-h posterior mean $\pm 1\sigma$	5-h posterior mean $\pm 1\sigma$
Azusa	0.240	0.214	0.167	0.185 ± 0.065	0.199 ± 0.042	0.168 ± 0.033
Riverside	0.240	0.196	0.246	0.185 ± 0.044	0.191 ± 0.034	0.177 ± 0.031

As discussed in the previous section, posterior probabilities, p'_k, for each Monte Carlo run can also be applied to the sampled input and parameter values used in that run, to update the estimates of these values. Table 3 shows the input variables whose estimated probability distributions are modified most by the Bayesian updates, as measured by the differences between the prior and posterior mean values. Posterior estimates based on the final-h likelihood function and those based on the 5-h likelihood function both show the largest change for the parameter AFG2 + *hv*, which is the photolysis rate of the unknown fragmentation products of aromatics oxidation. The mean value of this rate constant is increased by about 10% when the final likelihood function is used; and decreased by about 15% when the 5-h likelihood function is used. The AFG2 photolysis rate has a strong influence on the O_3 concentration (Yang et al., 1995), and was also assigned a relatively large prior uncertainty (Stockwell et al., 1994). The second largest change resulting from use of the final likelihood function is an increase of about 5% in the rate constant for PPN decomposition. Changes in the mean values of other parameters with the final likelihood function are less than about 3%. With the 5-h likelihood function, the estimated mean rate constant for PAN decomposition is decreased by about 8%, and mean values for four other parameters are reduced by 5–6%. Overall, however, adjustments to the mean values and standard deviations of the input parameters from the Bayesian analysis are small.

Table 4 presents a comparison of prior and posterior correlations between selected input parameters and the final O_3 concentrations at Azusa and Riverside. The prior correlations reflect the sensitivity of the final O_3 concentrations to independent variations in each parameter. In contrast, the posterior correlations are affected by correlations between parameters that are induced by the different posterior probabilities of each sample. As shown in Table 4, both 5-h and final-h posterior correlations are lower than the prior correlations of final O_3 concentrations with motor vehicle emissions, trajectory path emissions, the O_3 deposition affinity and the rate parameters for NO_2 + OH, RCO3 + NO, and PAN decomposition. Five-h posterior probabilities increase the correlations between the final O_3 concentration at Azusa and the rate constants for both $O(1D) + H_2O$ and O(1D) + M and between the final O_3 concentration at Riverside and the AFG2 + *hv* rate parameter. The 5-h posterior probabilities reduce the correlation between the NO_2 + *hv* rate parameter and the final O_3 concentration at Riverside by nearly a factor of two, but increase its correlation with the final O_3 concentration at Azusa.

In addition to the correlation of input parameters with final ozone concentrations, prior and posterior correlation coefficients were examined for pairs of input parameters. The prior correlation coefficients for the input parameters are generally less than 0.05 as desired for independent variables generated with LHS. A positive induced correlation indicates that observed concentrations are matched best when the parameters deviate from their mean values in the same direction. In contrast, a negative correlation indicates that observed concentrations are best matched if an increase in the value of the first parameter is accompanied by a decrease in the second one, or vice versa.

Among the input parameters listed in Table 4, the largest degrees of correlation induced by the 5-h posterior probabilities are: 0.26 and 0.24 for the rate parameter of NO_2 + HO with the Riverside and Azusa trajectory emissions, respectively; -0.23 for the NO_2 photolysis rate and the Riverside trajectory emissions; -0.22 for motor vehicle emissions and the Azusa trajectory emissions; and 0.21 for the rate parameters of $O(1D) + H_2O$ and NO_2 photolysis. The largest degrees of correlation induced by the final-h posterior probabilities are: 0.16 and 0.12 for the NO_2 + HO rate parameter with the Riverside and Azusa trajectory emissions, respectively; -0.12 for Riverside trajectory emissions with the rate parameter for PAN decomposition; and -0.12 for motor vehicle emissions with the RCO3 + NO rate parameter.

The induced correlation between pairs of input parameters helps explain the changes in correlation between the input parameters and the output O_3 concentrations. For example, the influence of the motor vehicle emissions input is reduced by its positive correlation with the $O(1D) + M$ rate constant ($\rho = 0.18$) and its negative correlation with Azusa trajectory path emissions

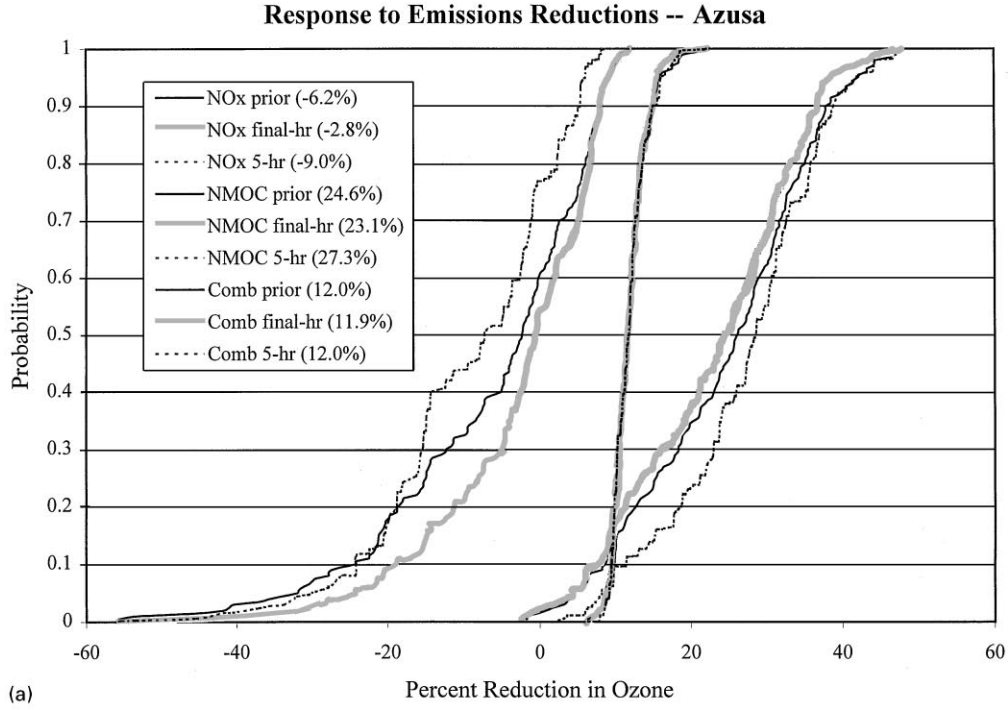

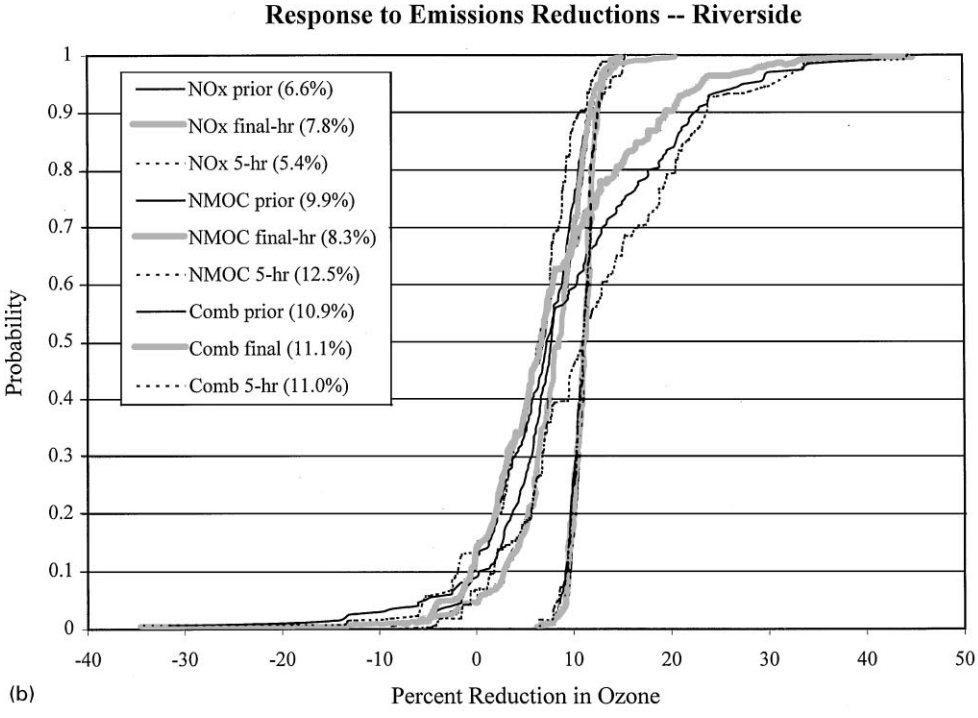

Fig. 3. Prior and posterior cumulative probability distributions of percentage reductions in peak ozone due to 25% reductions in motor vehicle emissions of NO_x, NMOC or NO_x and NMOC combined. (a) Reductions in O_3 at Azusa. (b) Reductions in O_3 at Riverside. The mean estimates are shown in the legends in parentheses. In the legends, NO_x prior refers to prior Monte Carlo results of the case with a 25% reduction in motor vehicle NO_x emissions. NO_x final-h and NO_x 5-h are the posterior estimates obtained for that case with the final-h and 5-h likelihood functions applied, respectively. The labels for the cases with 25% reductions in motor vehicle NMOC emissions and combined reductions (Comb) are defined in the same way.

Table 3
Effect of Bayesian updating on estimates of model inputs and parameters. Results are shown for the six parameters exhibiting the largest changes in the mean value when both the final- and 5-h posterior probabilities are applied to each input sample

Final-h posterior				5-h posterior			
Variable	Prior COV	% Change in μ	% Change in σ	Variable	Prior COV	% Change in μ	% Change in σ
AFG2 + *hv*	1.33	10.4	4.9	AFG2 + *hv*	1.33	− 15.4	5.8
PPN	0.80	4.8	4.0	PAN	0.39	− 8.3	− 12.5
RCO3 + NO	0.34	3.0	7.4	RO2R + NO	0.42	− 6.1	− 9.0
MV_emis	0.25	2.3	− 5.8	PPN	0.80	− 5.4	− 10.6
NO_2_aff	0.29	2.3	1.1	MV_emis	0.25	− 5.2	3.4
O_3_aff	0.29	− 2.0	− 0.5	HCHO + *hv*	0.34	− 5.0	− 7.0

Table 4
Correlation of selected input parameters with modeled final ozone concentrations at Azusa and Riverside

	Azusa			Riverside		
	Prior	5-h posterior	Final-h posterior	Prior	5-h posterior	Final-h posterior
MV_emis	0.45	0.22	0.30	0.43	0.28	0.29
NO_2 + OH	− 0.32	− 0.23	− 0.21	− 0.18	− 0.09	− 0.13
CO_traj[a]	0.32	0.13	0.24	0.45	0.33	0.33
NO_2 + *hv*	0.29	0.38	0.27	0.31	0.12	0.24
RCO3 + NO	0.24	0.12	0.19	0.31	0.16	0.24
PAN	0.21	0.20	0.11	0.15	0.15	0.04
AFG2 + *hv*	0.20	0.25	0.17	0.07	0.14	0.02
O_3_aff	− 0.19	− 0.08	− 0.06	− 0.26	− 0.04	− 0.14
O(1D) + H_2O	0.11	0.27	0.11	0.00	− 0.03	− 0.03
O(1D) + M	− 0.05	− 0.16	− 0.05	0.01	− 0.04	0.00

[a]Sum of CO emissions along each trajectory for either Azusa or Riverside.

($\rho = -0.22$) and the rate constant for RCO3 + NO ($\rho = -0.18$). The influence of the NO_2 photolysis rate at Riverside is reduced by its negative correlation with emissions along different Riverside trajectories.

The posterior probabilities were also applied to Monte Carlo simulation results in which NO_x, NMOC, and combined NO_x and NMOC emissions from motor vehicles were reduced by 25%. In effect, this weight each prediction according to how well the corresponding base case simulation matched the interpolated observations. Fig. 3 shows prior and posterior cumulative distribution functions of the percentage reduction in O_3 achieved with each of these cases.

At Azusa, the prior and posterior model results are consistent in indicating that reductions in NMOC emissions would be more effective than reductions in NO_x emissions, which have a substantial probability of increasing final ozone concentrations. Posterior estimates based on the final-h likelihood function make NO_x emissions reductions appear slightly more effective and NMOC emissions reductions slightly less effective than the prior estimates, but the shifts are not large. The 5-h likelihood function has the opposite impact, favoring NMOC reductions. The estimated effect of combined reductions in NMOC and NO_x emissions has relatively little prior uncertainty, and the posterior distributions for this case are almost identical to the prior distributions.

At Riverside, the means of the prior and final-hr posterior distributions suggest that reducing NMOC emissions would be more effective than reducing NO_x emissions, but the median (50th percentile) results suggest the opposite. Both the means and the median estimates from the 5-h posterior distributions show NMOC reductions as being more effective than NO_x reductions. As at Azusa, there is little uncertainty and negligible effect of Bayesian updating on the predicted response to combined reductions in NMOC and NO_x emissions.

4. Discussion

For the cases studied here, the prior Monte Carlo results and interpolated observations were in reasonable agreement. Consequently the Bayesian analysis reduces Bergin et al.'s (1999) estimates of uncertainties in base case O_3 concentrations at Azusa and Riverside from 35 and 24% to about 20 and 18%, respectively. Updates using the 5-h likelihood function make NMOC emissions reductions appear somewhat more effective, and NO_x reductions somewhat less effective than indicated by the prior Monte Carlo results. However, these findings are specific to the model, simulation conditions, observations and error estimates used in this study.

An important limitation of Bayesian Monte Carlo analysis is the underlying assumption that all of the significant sources of uncertainty in the model are accounted for in the prior Monte Carlo analysis. The trajectory model used in this study neglects wind shear and horizontal diffusion, which introduces errors associated with model structure that have not been treated in the Monte Carlo analysis. In addition, Bergin et al.'s study only accounted for uncertainties in total emissions from various sources, not uncertainties in their spatial and temporal distribution. Due to these limitations, this study should be viewed primarily as a demonstration of the Bayesian Monte Carlo technique. In future studies, BMC should be applied to a detailed three-dimensional airshed model to minimize the uncertainty due to model structure.

A second limitation of this study is that only O_3 data were used in the Bayesian updating step. Incorporation of NMOC and NO_x measurements as well as observations of other photochemical products would be useful to further refine Bayesian updates of input parameter values and model predictions. However, care needs to be taken in estimating likelihood functions for these additional species. For example, the mismatch between interpolated point measurements and grid-cell-averaged model results is expected to be even more pronounced for NMOC or NO_x concentrations than for O_3.

As shown here by the comparison of Bayesian updates made with the final- versus 5-h likelihood functions, the results of Bayesian Monte Carlo analysis can be sensitive to the choice of observations incorporated in the analysis. For example, the 5-h and final-h likelihood functions nudge the mean estimate of the AFG2 + $h\nu$ rate parameter in opposite directions. In addition, the 5-h likelihood function makes NMOC emissions reductions appear relatively more effective whereas the final-h likelihood tends to improve the predicted effectiveness of NO_x reductions. In this study, posterior estimates based on the 5-h likelihood function are judged to be more reliable than those based on the final likelihood function, because they utilize more information from the observations. Use of the 5-h likelihood function is also in keeping with recent interest in an 8-h O_3 standard. The Markov chain likelihood function was limited to a 5-h time period because earlier O_3 concentrations drop below the 60 ppb cutoff for which McNair et al. (1996) performed the interpolation error analysis. In future work, the error analysis could be extended to lower concentrations to allow longer time series to be used for Bayesian updating. Additionally, if BMC were applied to a three-dimensional model, observations could be incorporated from more sites.

Ideally, confidence levels placed on model predictions should reflect both prior information about input and parameter uncertainties and information about model performance. Provided that the likelihood function can be adequately defined, BMC analysis appears to be a useful technique for combining these two types of information. In future studies, BMC should be applied to three-dimensional air quality models, because of their widespread use in designing control strategies for urban ozone.

Acknowledgements

The authors would like to thank Greg Noblet, Rob Harley and Laurie McNair for essential contributions to this study, and Mitch Small for a helpful review of the manuscript. The work was supported by the U.S. Environmental Protection Agency, assistance agreement R 824797-01-0.

References

Beck, M.B., 1987. Water quality modeling: a review of the analysis of uncertainty. Water Resources Research 23, 1393–1442.

Bergin, M.S., Noblet, G.S., Petrini, K., Dhieux, J.R., Milford, J.B., Harley, R.A., 1999. Formal uncertainty analysis of a Lagrangian photochemical air pollution model. Environmental Science and Technology 33, 1116–1126.

Benjamin, J.R., Cornell, C.A., 1970. Probability, Statistics and Decision for Civil Engineers. McGraw-Hill, New York, p. 322.

Brand, K.P., Small, M.J., 1995. Updating uncertainty in an integrated risk assessment: conceptual framework and methods. Risk Analysis 15, 719–731.

Carter, W.P.L., 1995. Computer modeling of environmental chamber measurements of maximum incremental reactivities of volatile organic compounds. Atmospheric Environment 29, 2513–2527.

Chock, D.P., 1984. Statistics of extreme values of a first-order Markov normal process: an exact result. Atmospheric Environment 18, 2461–2470.

Dakins, M.E., Toll, J.E., Small, M.J., Brand, K.P., 1996. Risk-based environmental remediation: Bayesian Monte Carlo analysis and the Expected Value of Sample Information. Risk Analysis 16, 67–79.

Dilks, D.W., Canale, R.P., Meier, P.G., 1992. Development of Bayesian Monte Carlo techniques for water quality model uncertainty. Ecological Modelling 62, 149–162.

Gao, D., Stockwell, W.R., Milford, J.B., 1996. Global uncertainty analysis of a regional scale gas-phase chemical mechanism. Journal of Geophysical Research 101, 9107–9119.

Goodin, W.R., McRae, G.J., Seinfeld, J.H., 1979. A comparison of interpolation methods for sparse data: application to wind and concentration data. Journal of Applied Meteorology 18, 761–771.

Guttman, I., Wilks, S.S., Hunter, J.S., 1982. Introductory Engineering Statistics. Wiley, New York, p. 510.

Hanna, S.R., Chang, J.C., Fernau, M.E., 1998. Monte Carlo estimates of uncertainties in predictions by a photochemical grid model (UAM-IV) due to uncertainties in input variables. Atmospheric Environment 32, 3619–3628.

Harley, R.A., Sawyer, R.F., Milford, J.B., 1997. Updated photochemical modeling for California's South Coast Air Basin: comparison of chemical mechanisms and motor vehicle emission inventories. Environmental Science and Technology 31, 2829–2839.

Harley, R.A., 1998. Personal communication, Department of Civil Engineering, University of California, Berkeley, CA, May.

Hornberger, G.M., Spear, R.C., 1980. Eutrophication in Peel Inlet 2: identification of critical uncertainties via generalized sensitivity analysis. Water Research 14, 43–49.

Iman, R.L., Shortencarier, M.J., 1984. A FORTRAN 77 program and users guide for the generation of Latin hypercube and random samples for use with computer models. NUREG/CR-3624; Sandia National Laboratories, Albuquerque, NM, March.

Lawson, D.R., 1990. The Southern California air quality study. Journal of the Air and Waste Management Association 40, 156–165.

McNair, L.A., Harley, R.A., Russell, A.G., 1996. Spatial inhomogeneity in pollutant concentrations, and their implications for air quality model evaluation. Atmospheric Environment 30, 4291–4301.

McRae, G.J., Seinfeld, J.H., 1983. Development of a second generation mathematical model for urban air pollution: II. Evaluation of model performance. Atmospheric Environment 17, 501–522.

Noblet, G., Harley, R., Dhieux, J., Milford, J.B., 1998. Effect of wind field uncertainty on predictions of a Lagrangian photochemical air quality model, 98-RA76B.02. Proceedings of the 91st Annual Meeting of the Air and Waste Management Association, San Diego, CA, 14–18 June.

Pandis, S.N., Harley, R.A., Cass, G.R., Seinfeld, J.H., 1992. Secondary organic aerosol formation and transport. Atmospheric Environment 26A, 2269–2282.

Patwardhan, A., Small, M.J., 1992. Bayesian methods for model uncertainty analysis with application to future sea level rise. Risk Analysis 12, 513–523.

Romanowicz, R., Higson, H., Teasdale, I., Lowles, I., 1998. Uncertainty estimation of an air pollution model. In: Gryning, S.E., Chaumerliac, N. (Eds.), Air Pollution Modeling and its Application XII. Proceedings of the Twenty-Second NATO/CCMS International Technical Meeting on Air Pollution Modeling and its Application. Clermont-Ferrand, France, 2–6 June 1997, Plenum Press, New York.

Russell, A.G., McRae, G.J., Cass, G.R., 1983. Mathematical modeling of the formation and transport of ammonium nitrate aerosol. Atmospheric Environment 17, 949–964.

Sohn, M.D., Small, M.J., Pantazidou, M., 1999. Updating uncertainty in site characterization and chemical fate and transport in groundwater (in preparation).

Stockwell, W.R., Yang, Y.-J., Milford, J.B., 1994. A compilation of estimated uncertainty factors for rate constants in W.P.L. Carter's detailed mechanism. Auto/Oil Air Quality Improvement Research Program, October.

Tesche, T.W., 1988. Accuracy of ozone air quality models. Journal of Environmental Engineering 114, 739–752.

Yang, Y.-J., Stockwell, W.R., Milford, J.B., 1995. Uncertainties in incremental reactivities of volatile organic compounds. Environmental Science and Technology 29, 1336–1345.